Physical interpretation of the floating electrode defect patterns under AC and DC stress conditions

Madhar, Saliha Abdul; Mraz, Petr; Mor, Armando Rodrigo; Ross, Robert

DOI
10.1016/j.ijepes.2019.105733

Publication date
2019

Document Version
Final published version

Published in
International Journal of Electrical Power & Energy Systems

Citation (APA)
Madhar, S. A., Mraz, P., Mor, A. R., & Ross, R. (2019). Physical interpretation of the floating electrode defect patterns under AC and DC stress conditions. *International Journal of Electrical Power & Energy Systems*, *118*, 1-8. Article 105733. https://doi.org/10.1016/j.ijepes.2019.105733

Electrical Power and Energy Systems 118 (2020) 105733

Contents lists available at ScienceDirect

Electrical Power and Energy Systems

journal homepage: www.elsevier.com/locate/ijepes

Physical interpretation of the floating electrode defect patterns under AC and DC stress conditions

Saliha Abdul Madhar[a,b,*], Petr Mraz[b], Armando Rodrigo Mor[a], Robert Ross[a]

[a] Delft University of Technology, Mekelweg 4, 2628 CD Delft, the Netherlands
[b] Haefely AG, Birsstrasse 300, 4052 Basel, Switzerland

ARTICLE INFO

Keywords:
Floating electrode
Defect
Corona
Partial discharge (PD)
Patterns
HVDC

ABSTRACT

Partial discharge is a prevalent phenomenon under high voltage (HV) where the discharge partially bridges the gap between two electrodes. At increasing voltage levels, physical dimensions and distances between the electrical parts become critical. Designing electrical components for such high voltages and planning of high voltage laboratories/tests need to deliberate this aspect as it could lead to possible complications such as partial discharges (PD) from the floating metal components. Floating electrodes under AC voltages are associated with a distinctive PRPD pattern. However, there is a lack of literature on the physical interpretation of this pattern. Likewise, under DC voltages, no consistent explanation towards the defect behavior has been reported. Therefore, this paper presents an in-depth study of the floating electrode defect configuration under AC and DC voltages. Subsequently, it provides the physical interpretation of the discharge patterns obtained through the stepwise description of the discharge stages under both conditions. By formulating criteria for repetitive discharges and presenting novel PD fingerprints for DC floating electrode configuration, the outcomes published in this paper contribute towards prospective PD defect identification tools under HVDC.

1. Introduction

Floating electrode at high voltages (HV) refers to a metallic object in the vicinity of an electric field that acquires a stray voltage depending on the level of capacitive coupling. If the voltage acquired by the metallic body is sufficient to cause a partial flashover to the main electrode, ground or initiate corona around the body, then the partial discharge from the floating electrode appears. This phenomenon also occurs in nature in the event of a thunderstorm/lightning. The electric fields during a thunderstorm can induce charges on ungrounded metallic bodies, causing them to discharge. These aspects of floating body discharge in a lightning protection system have been studied in [1–4]. The risk involved with floating bodies in HV systems is manifest through the possibility of shock and flashover. The level of risk depends on the energy held across the floating body (capacitive energy). On account of this, HV installations always specify clearances, which are distances at which it is safe for personnel to operate other equipment [5]. A Floating PD from an external source in more specific can stall the progress of quality inspection and qualification in test laboratories. And an internal floating defect in the dielectric of the component risks the weakening of the dielectric depending the level/nature of discharge.

In AC tests, the modern-day partial discharge (PD) measuring equipment creates a Phase Resolved Partial Discharge (PRPD) pattern during the test which allows defect identification [6]. It is the unique shape of this PRPD pattern that helps in the identification of the defect as it holds the information about the defect's behavior. Though the various trends of discharge progression with increasing voltage and time have been studied, little has been known so far on the actual interpretation on the pattern itself. This paper aims at shedding light on the physical interpretation of the PRPD pattern of the floating electrode defect through the identification of key features of the defect behavior. This is systematically done by plotting several discharge parameters. Following that, the paper provides the detailed and stepwise description of the discharge behavior.

On the other hand, in the case of DC, several researchers have studied the discharge characteristics and presented the resultant patterns of floating particles or free-moving particles since this is of interest for Gas Insulated Systems (GIS) [7,8]. However, there is a lack of literature that describes the floating electrode defect similar to AC conditions. Hence, this contribution presents a detailed study of the discharge process from a floating electrode defect by identifying various discharge characteristics that represent the defect accurately. Further, the criteria for the repetitive stage of discharge from a floating electrode are defined and DC-PD fingerprints for the defect are presented.

* Corresponding author.
E-mail address: S.AbdulMadhar@tudelft.nl (S. Abdul Madhar).

https://doi.org/10.1016/j.ijepes.2019.105733
Received 4 July 2019; Received in revised form 19 November 2019; Accepted 22 November 2019

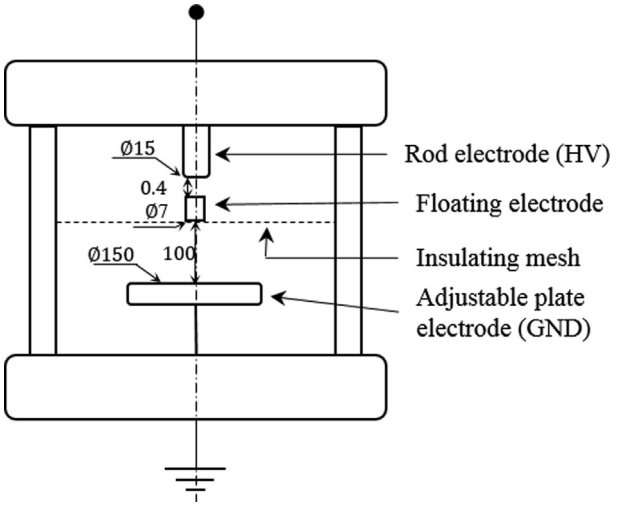

Fig. 1. Schematic of the floating electrode defect arrangement (all dimensions are in mm).

The contributions of the paper could be subsequently utilized for defect identification under HVDC and as an extension of the existing knowledge in the field of AC partial discharges.

2. Experimental setup

To reproduce a floating electrode defect, a set-up with a floating metallic electrode is constructed using a rod-plate arrangement (main electrodes) as shown in Fig. 1. The electrode is held in a floating position with the help of an insulating mesh. The distance between the floating electrode and the rod electrode at HV is kept at 0.4 mm, while its distance to the ground electrode is maintained at 100 mm. The other dimensions are specified in Fig. 1. The floating electrode has a small extension on the lower part to allow field enhancement which helps demonstrate the feature of corona from floating electrode. The defect arrangement is placed in open air at atmospheric pressure of 1 atm.

The PD measurement setup in case of AC was built according to the IEC 60270 [9], with a coupling capacitor (C_k), quadrupole (Z_m) and a PD detector. The schematic of the measuring setup is shown in Fig. 2. Fig. 3 shows the schematic of the DC PD measurement setup. The half-wave rectifier is used to rectify the HVAC source, the direction of the diode determines the polarity of rectified DC. A resistive divider is used in parallel with the test object to measure the DC voltage. The PD

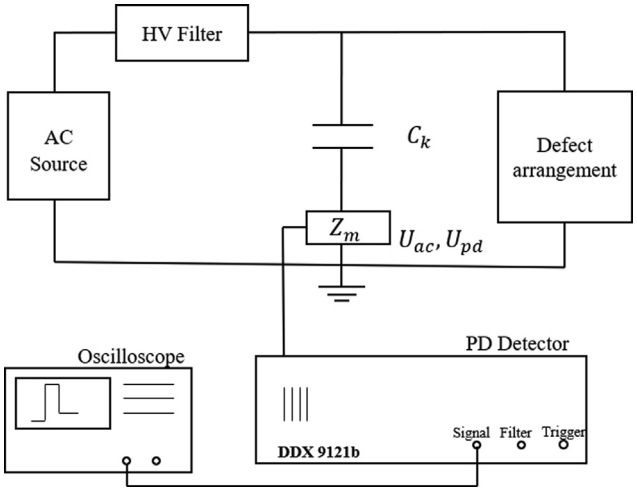

Fig. 2. Schematic of the AC PD measuring setup built according to IEC 60270 [9].

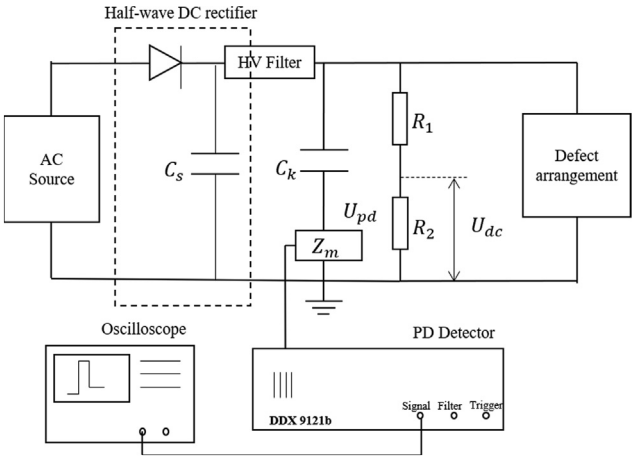

Fig. 3. Schematic of the PD measuring setup used for the study of floating electrode defect configuration under DC.

measurements are made by two means. Firstly, through the PD detector (DDX 9121b) which logs the voltage, charge (pC), repetition rate and pulse polarity every second. This provides a real time estimate of the partial discharge events. And secondly, using an oscilloscope with a measuring bandwidth (BW) of 250 MHz that is fed through the 'signal' output channel on the DDX 9121b [10]. The oscilloscope records a continuous data stream at the rate of 20 MS/s. Continuous data streaming reduces the probability of errors during acquisition and provides the possibility of reviewing the raw-data stream during the post-processing phase. The streamed raw data is independent of the IEC filter settings defined in the detector but is influenced by the detector's amplifier stage. In order to tackle this, the amplification level is set to a fixed value. A set of specially developed algorithms on Matlab software are used for post-processing to generate the resultant discharge patterns.

3. Floating electrodes under AC voltages

The floating electrode defect under AC voltages is most commonly associated with its distinctive PRPD pattern as shown in Fig. 4 [11]. A stable, repetitive stage of discharge for the configuration under test is reached at 9.50 kV_{rms} establishing this as the PD inception voltage (U_i or PDIV). The discharge magnitude remains fairly constant over a given voltage and moves predominantly Fig. 6 over the rising edge of the positive and negative half-cycle creating the straight lines over the PRPD pattern. When looking at the discharge pulse occurrence carefully one will notice the sliding of the pulse over the voltage phase towards and away from each other. This has been pictorially demonstrated through Fig. 5. This phenomenon is a characteristic feature of a floating electrode defect and can alternatively be recognized or studied through

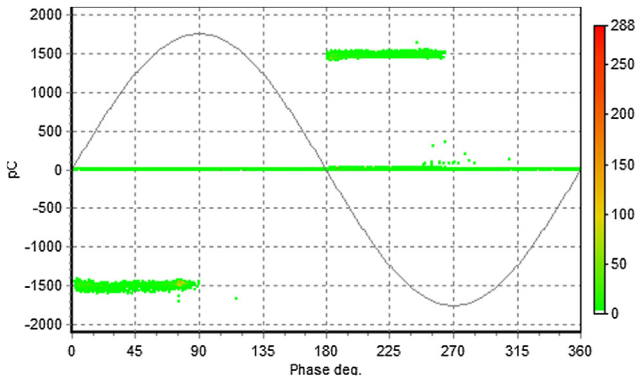

Fig. 4. PRPD pattern of a typical floating electrode defect.

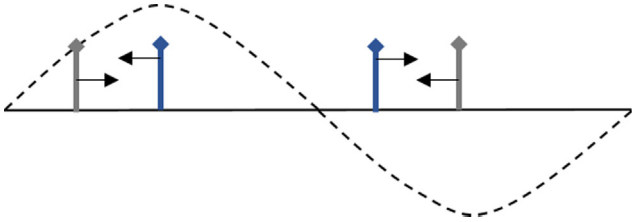

Fig. 5. Pictorial representation of the moving pulse in a typical floating electrode defect.

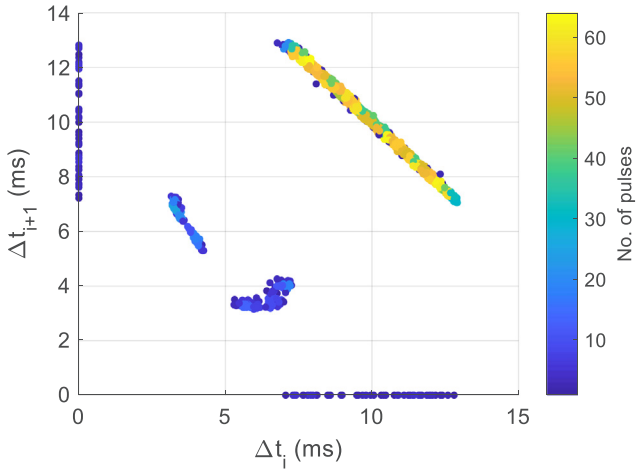

Fig. 6. The plot of time between successive discharges of a 3-pulse sequence for a typical floating electrode defect.

the 3-pulse PSA (Pulse Sequence Analysis) plot of time between successive discharges as shown in Fig. 6 [12].

The 3-pulse PSA plot of time between successive discharges shows a linear curve that extends between the coordinates of (7,13) ms and (13,7) ms. This illustrates that the time between the 2 discharges on the 2 half-cycle changes between 7 and 13 ms and follows a well-defined sequence. It also depicts that there are just 2 discharges per voltage cycle (20 ms or 50 Hz) as the sum of two successive Δt yields 20 ms, which is the time period of a 50 Hz cycle. For instance, the cluster around 4–6 ms seen in Fig. 6 depicts the discharge period when there occur more than 2 pulses per cycle.

To further understand the sequence in the change of time between successive discharges (Δt), the bar graph of the same is presented in Fig. 7. This clearly shows the sequential increase (from 7 to 13 ms or 126° to 234°) and subsequent decrease (from 13 to 7 ms) of the time between discharges. Concurrently, one can also observe a region with Δt ranging from 4 to 6 ms. This is the period of discharge with 4 pulses per voltage cycle. Here, the sum of 4 successive Δt yields the time period of the 50 Hz cycle (20 ms). This region indicates that there are 2 discharges per half-cycle. Typically, in the case of floating electrode defects, with an increasing level of voltage above discharge inception, multiple pulses per half-cycle can be observed. Whereas the level of discharge magnitude remains constant. This is because the discharge magnitude is related to the gap withstand voltage and given that the floating body is fixed, the resultant PD magnitude remains constant. However, once the voltage exceeds the corona inception level for the curvature of the floating body, corona can also be observed. Section 3.2 is dedicated to the description of this phenomenon in more detail.

3.1. Defect behavior

The reason for this unique feature of floating electrode discharge in which the pulses move towards and away from each other over the voltage phase lies in its physics. Therefore, the following section

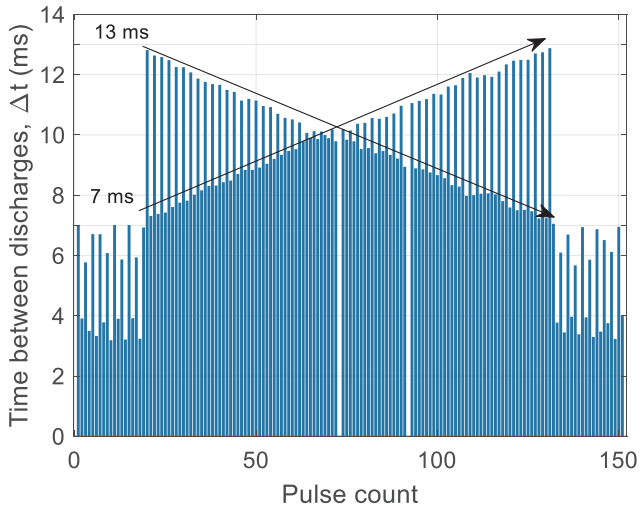

Fig. 7. The plot of time between discharges for the floating electrode defect under AC voltage.

provides a theoretical background to the stepwise behavior of a floating electrode defect under AC voltage cycle.

For illustration, let us consider a homogenous electric field distribution between two conducting plate electrodes with the floating electrode placed at a distance 'l' from the electrode at HV, as shown in Fig. 8a. Based on the capacitive coupling to the electrode arrangement the floating electrode acquires a certain voltage that is equivalent to;

$$V(\omega) = E_f(\omega) \cdot l \tag{1}$$

where E_f is the electric field intensity across the gap distance with length l, and is a sum of the electric field from the applied voltage ($E_{ext}(\omega)$) and the field from the induced charges over the floating electrode ($E_s(\omega)$). All the field and voltage values are a function of the angular frequency, ω of the power supply. Initially, the net charge on the metallic floating body remains zero (electrically neutral). Once the acquired voltage exceeds the gap withstand voltage, over the positive half-cycle, the voltage across the gap 'l' reaches the breakdown value thereby bridging the gap momentarily by a spark discharge or a current path. In terms of partial discharge measurements, it is represented as a current pulse with an integral equivalent to;

$$\Delta Q = \bar{i} \cdot \Delta t \tag{2}$$

where $\bar{i}$ is the mean value of current, $\Delta t$is the transient time of the discharge process and ΔQ is the value of charge. The discharge magnitude is a function of the electric field intensity (E_f) at the gap and the level of capacitive coupling of the floating electrode which in turn depends on the area of the floating electrode, the gap distance and the permittivity of the dielectric. The initial phase until and including the first breakdown can be described by the following set of equations;

$$At \quad t = t_o,$$

$$V_{ind} = \widehat{V}_{ind} \sin(\omega t_o + \varphi) \tag{3}$$

$$V_{ext} = \widehat{V}_{ext} \sin \omega t_o \tag{4}$$

$$V_{bd} = V_{ext} + V_{ind} \tag{5}$$

where V_{ind} is the induced voltage on the floating electrode which follows the supply voltage, V_{ext} is the voltage drop across gap 'l' due to the applied voltage, $\widehat{V}_{ind}$ and $\widehat{V}_{ext}$ are the absolute peak values of the voltage and V_{bd} is the breakdown voltage of the gap 'l', φ is the phase shift between the induced voltage, V_{ind} and the external voltage drop V_{ext} arising from the capacitive nature of the floating gap.

The transient phase of the discharge brings the floating electrode to the HV electrode's potential momentarily, charging it positively (due to

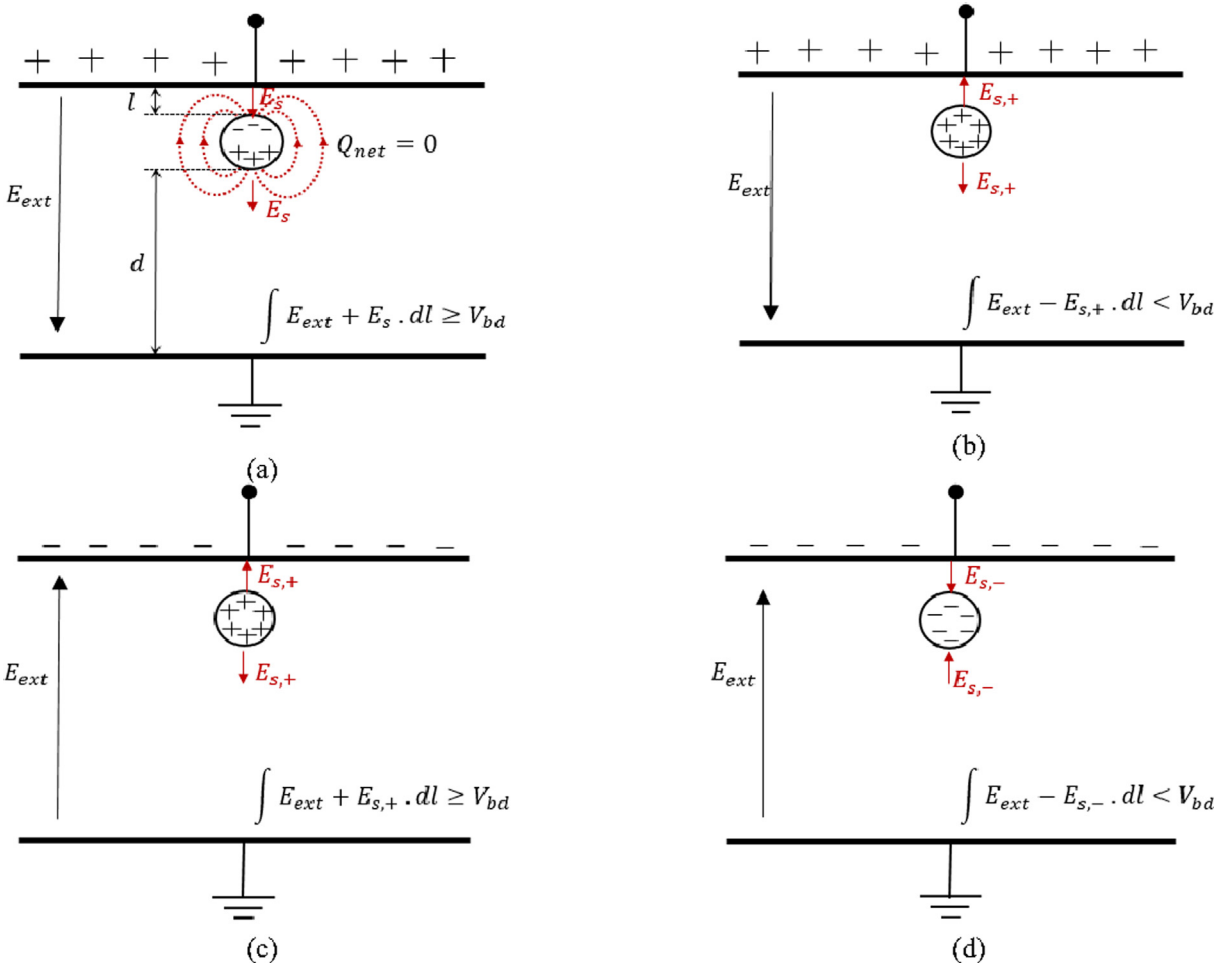

Fig. 8. Schematic of the stepwise discharge process of a floating electrode defect under AC voltage (a) floating body before first breakdown of gap '*l*' during positive half-cycle (b) after first breakdown of gap '*l*' during positive half-cycle (c) before breakdown of gap '*l*' in the subsequent negative half-cycle and (d) after breakdown of gap '*l*' during the negative half-cycle.

the positive half-wave). Therefore, now the floating electrode is no more electrically neutral but possess a charge equivalent to 'q' given in Eq. (6). Based on the electrical field drawings shown in Fig. 8b it can be observed that the applied electric field (E_{ext}) due to the supply voltage and the static electric field ($E_{s,+}$) due to the charge on the floating electrode now oppose one another in the gap 'l' and hence the defect does not discharge again over the positive half-cycle given the voltage drop due to $E_{s,+}$ compensates for the sinusoidal increase in the applied AC voltage. When the AC voltage polarity changes to the negative half-wave, the scenario Fig. 8c occurs, where the applied electric field (E_{ext}) and the static electric field ($E_{s,+}$) add constructively once again to exceed the value of breakdown voltage of gap 'l' initiating a discharge at $t = t_1$. The following equations describe the moment preceding the discharge event at $t = t_1$;

$$q = C \cdot V_{bd}(t_o) \tag{6}$$

$$E_{s,+}(t_1) = \frac{k.\,q}{l^2} \tag{7}$$

$$V_{s,+}(t_1) = E_{s,+}(t_1) \cdot l \tag{8}$$

$$V_{bd}(t_1) = V_{ext}(t_1) + V_{ind}(t_1) + V_{s,+}(t_1) \tag{9}$$

$$= \widehat{V}_{ext}\sin\omega t_1 + + \widehat{V}_{ind}\sin(\omega t_1 + \varphi) + \frac{kC}{l}[\widehat{V}_{ext}\sin\omega t_o + \widehat{V}_{ind}\sin(\omega t_o + \varphi)]$$

where q is the charge on the floating electrode after restoration of the gap resistance following the first discharge, C is its capacitance to the HV electrode, $V_{bd}(t_o)$ is the instantaneous voltage during the breakdown at $t = t_o$, $E_{s,+}$ is the electrostatic field due to charge q, k is the electrostatic constant equal to 8.99×10^9 Nm^2 C^{-2} and $V_{s,+}$ is the resultant electrostatic voltage. From Eq. (9) it can be resolved that the time (over half-cycle or phase position) t_1 at which discharge takes place depends on the voltage acquired as a result of the previous discharge at instance t_o. The discharge scenario based on Eq. (9) has been simulated for the purpose of demonstration and is shown in Fig. 9. It can be observed that since the breakdown at t_1 occurs at an increased voltage level (with reference to the external applied voltage, 0.84 V_{ext}) the discharge on the subsequent half-cycle at t_2 occurs at a lower level (0.30 V_{ext}). And this level of charge acquired at t_2 causes the discharge at t_3 to shift to a smaller voltage level (0.65 V_{ext}). Additionally, the sum of the subsequent values of Δt lie in the range of 19.05 and 20.50 ms which as in line with the observations presented in Section 3. One might otherwise also observe this time shifting of pulses over subsequent voltage-cycles as the sliding of the pulses away from each other (demonstrated through the arrows in Fig. 9). In sum, this confirms that the phase position at which the discharge takes place on one half-cycle determines the phase position of the subsequent discharge event on the next half-cycle.

3.2. Corona from floating electrode

Depending on the geometry and curvature of the floating electrode, corona may incept on it. The occurrence of corona before or after the

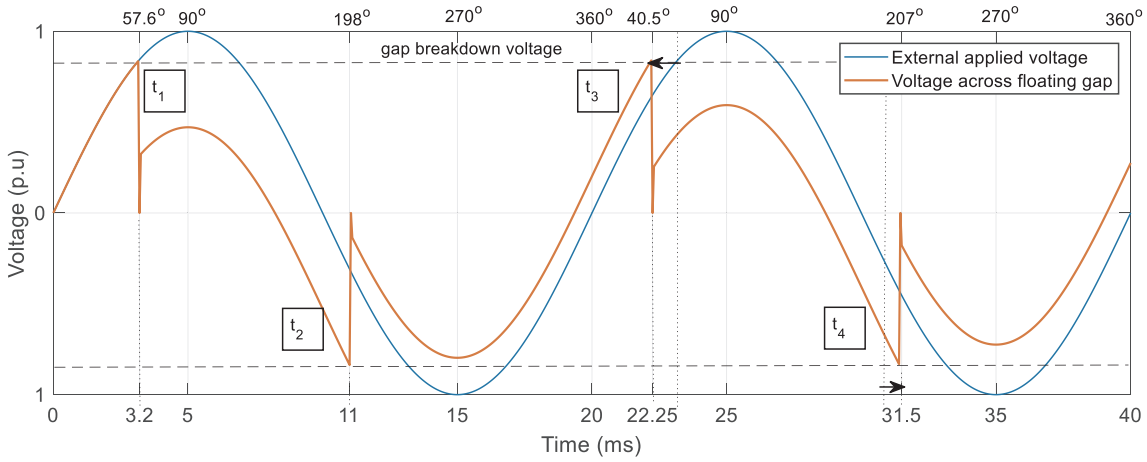

Fig. 9. Simulation of the floating defect discharge scenario demonstrated based on Eq. (9). The x-axis is given in terms of time in ms (below) and in terms of rotational phase in degrees (above).

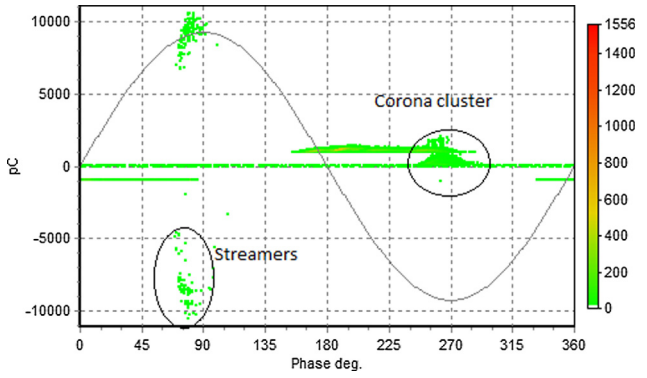

Fig. 10. PRPD pattern of the corona from the floating electrode defect.

floating stage purely depends on the geometry and positioning of the floating electrode in the gap. In the experimental case discussed in this paper, the corona from the floating electrode incepts with increasing voltage. The PRPD pattern of which is shown in Fig. 10. The difference between corona from a needle plate arrangement with the needle at HV and the corona coming from a floating electrode is the difference in the energy source. In case of the floating electrode, the energy on the floating electrode is given by:

$$W = \frac{1}{2} Q \cdot V \tag{11}$$

where Q is the charge on the floating electrode and V is the instantaneous voltage. Once the energy on the electrode is no more sufficient to incept the corona, the discharge ceases. Consider the floating electrode arrangement given in Fig. 8b, when the voltage is sufficiently high the positive charge acquired after breakdown by the floating electrode can incept positive corona (or streamers) over the gap '*d*'. As the floating electrode is electrically isolated, the positive corona charges the floating electrode negatively. With the floating electrode acquiring negative charge once again, the gap '*l*' breaks down making it positive again.

This process continues until polarity reversal. Similarly, at the negative half-cycle with increased voltage, negative corona incepts over gap '*d*'. The cluster shown in Fig. 10 over the positive polarity of the positive half-cycle is due to the incorrect polarity recognition by the PD detector due to insufficient vertical bit resolution as the streamer discharges are well above a few 10's of nC.

4. Floating electrodes under DC voltages

4.1. Under negative DC

The floating electrode defect under DC voltage follows a completely different sequence as compared to the AC defect. The defect in this case does not have a stable discharge repetition rate once the breakdown voltage of the gap '*l*' is reached. The first discharge over the gap takes place based on Eq. (5). In this case the values of V_{ind} and V_{ext} are equal to $\widehat{V}_{ind}$ and $\widehat{V}_{ext}$, given the DC voltage. However, after the first breakdown the electrode charges to a value of charge *q* given by Eq. (6). And due to the opposite orientation of the two fields (E_{ext} *and* $E_{s,-}$) similar to the orientation shown in Fig. 8d no further discharge takes place at this voltage level. The discharge over the gap recurs when the applied DC voltage increases by a value equivalent to;

$$\Delta V = (V_{s,-} + V_{ind}) \tag{12}$$

$$V_{s,-} = E_{s,-} \cdot l \tag{13}$$

where $V_{s,-}$ is the resultant voltage over the floating electrode as a consequence of the field $E_{s,-}$. With further increase in voltage, the sum of the applied electric field (E_{ext}) and the static electric field ($E_{s,-}$) leads to field enhancement over the gap '*d*' (scenario shown in Fig. 8d). This leads to inception of negative corona over the floating electrode. However, as mentioned in Section 3.2, due to the limited energy on the floating electrode the negative corona dies out or ceases leaving the floating electrode positively charged. To reach a stable discharge state the following two criteria need to be met:

i. The constructive overlap of the applied electric field (E_{ext}) and the static electric field ($E_{s,-}$) produces corona over gap '*d*'.
ii. The corona discharge charges the floating electrode in the opposite direction, increasing the field across gap '*l*' to the breakdown value.

Once, these two criteria are satisfied, a stable discharge can be observed. The results of the experiments performed substantiate this theory. This phenomenon of discharge can be observed in Fig. 11 where the pulses occur in blocks. The first pulse with larger amplitude is the breakdown of the gap '*l*', while the successive pulses with small amplitude are due to negative corona. This stage of the floating electrode discharge yields very distinct discharge patterns.

Fig. 12a shows the plot of difference in successive discharge magnitudes (ΔQ) vs. time between the successive discharges (Δt), Fig. 12b gives the plot of difference in discharge magnitudes of 2 pulses in a 3 pulse sequence (ΔQ_i *vs.* ΔQ_{i+1}) and Fig. 12c is a plot of time between successive discharges in a 3-pulse sequence (Δt_i *vs.* Δt_{i+1}). Fig. 12d is

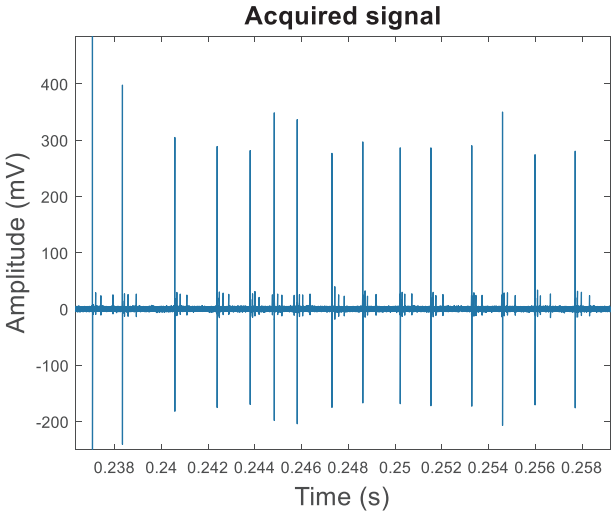

Fig. 11. Discharge stream recorded at $-29.5\ kV_{pk}$ with the floating electrode defect.

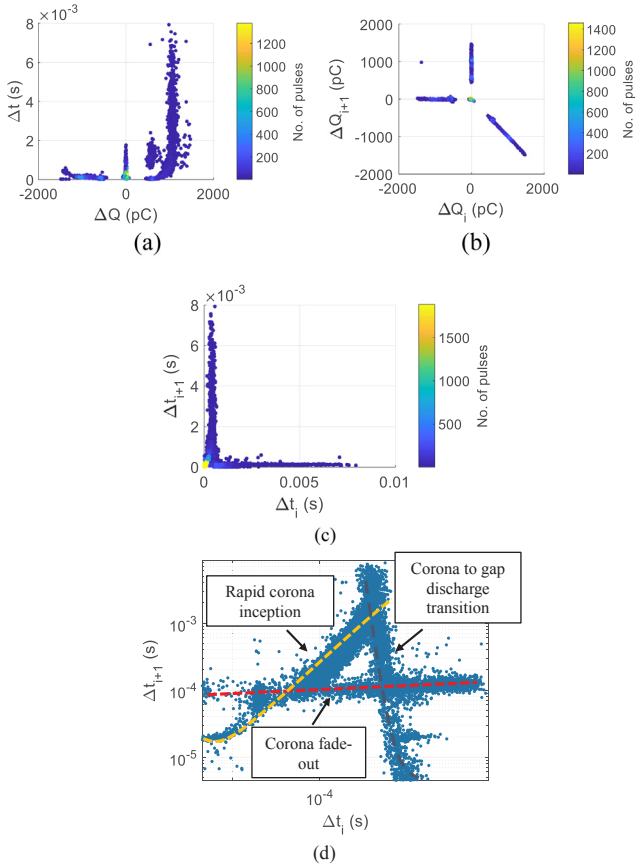

Fig. 12. PSA patterns of the floating electrode defect under $-29.5\ kV_{pk}$ (a) plot of difference in successive charge (ΔQ) vs. time between the successive discharges (Δt), (b) plot of difference in charge of 2 pulses in a 3-pulse sequence (ΔQ_i *vs.* ΔQ_{i+1}), (c) a plot of time between successive discharges in a 3-pulse sequence (Δt_i *vs.* Δt_{i+1}) and (d) Fig. 12c in logarithmic scaling.

the Fig. 12c presented in logarithmic scaling of the axis and excluding the heat map function. It is synonymous to Fig. 6 of the AC discharge pattern and shows a very distinct pattern similar to the one observed in the AC case. To further describe this pattern clearly, the bar graph of time between discharges of the floating electrode defect at the same voltage level is presented in Fig. 13.

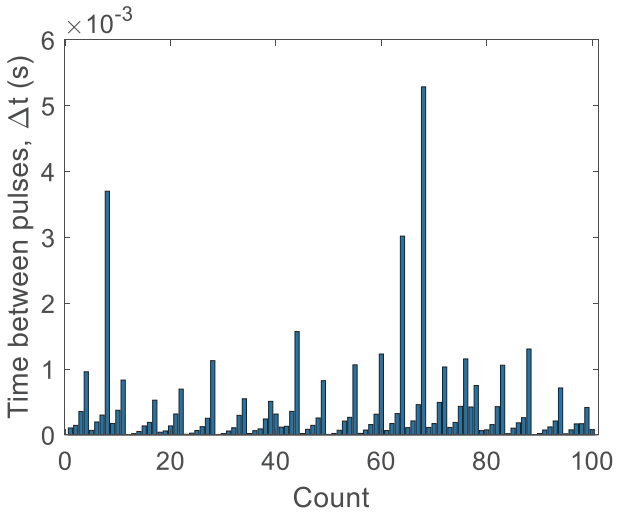

Fig. 13. The plot of time between discharges for floating electrode defect under -DC voltage of $-29.5\ kV_{pk}$.

From this it can be deduced that the time between discharges follows a very systematic scheme. The value of Δt increases exponentially from the discharge of gap '*l*' until the next discharge of gap '*l*'. The exponential curve shown by the yellow curve[1] in Fig. 12d indicate the corona inception over the floating electrode with small time between discharges. This can also be confirmed by the large density of pulses over this curve. The exponential decay curve shown by the black curve[1] indicates the discontinuity or the shift from the corona stage to the next discharge of gap '*l*'. The third prominent curve creating a stable line highlighted through the red line[1] in Fig. 12d indicates the slow repetitive corona towards its termination (corona fade-out).

4.2. Under positive DC

Under the positive polarity of the DC voltage. The floating electrode follows the sequence of steps shown in Fig. 8a and b. Once the gap breaks down and the floating electrode is charged positively, corona might incept on the floating body conditionally, when the criteria mentioned in Section 4.1 are satisfied. However, positive corona incepts at higher voltages than negative corona due to the absence of an electron source. Hence, the inception voltage of the repetitive discharge state of a floating electrode under positive DC is slightly higher than that under negative DC. After the first breakdown of the gap '*l*', several singular breakdowns can take place at increasing voltage steps given that the applied field E_{ext} increases sufficiently enough to compensate the previously accumulated positive charge.

Once the positive corona incepts over gap '*d*', the floating electrode begins to get charged in the opposite direction (negatively). The drop in the positive charge over the floating electrode increases yet again the field stress across gap '*l*', leading to the breakdown of the gap. Therefore, under the positive polarity there is a combination of streamer discharges and breakdown of the gap '*l*'.

The PSA plots associated with this configuration are shown in Fig. 14. The absence of the negative corona with the repetitive pulses does not give rise to the unique pattern over the PSA plot of time between pulses. The discharge pulse stream recorded under this configuration is shown in Fig. 15. From this, two types of pulses occurring alternatively can be observed, large and small. The discharge magnitude of the smaller pulses remains fairly constant while the larger pulses vary greatly. This feature of the discharge is reflected on the PSA

[1] For interpretation of color in Fig. 12, the reader is referred to the web version of this article.

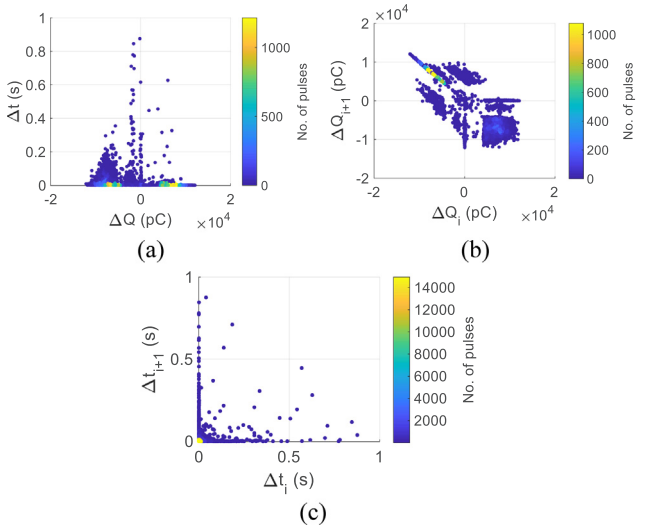

Fig. 14. PSA patterns of the floating electrode defect under +DC voltage (a) plot of difference in successive charge (ΔQ) vs. time between the successive discharges (Δt), (b) plot of difference in charge of 2 pulses in a 3-pulse sequence (ΔQ_i *vs.* ΔQ_{i+1}), (c) a plot of time between successive discharges in a 3-pulse sequence (Δt_i *vs.* Δt_{i+1}).

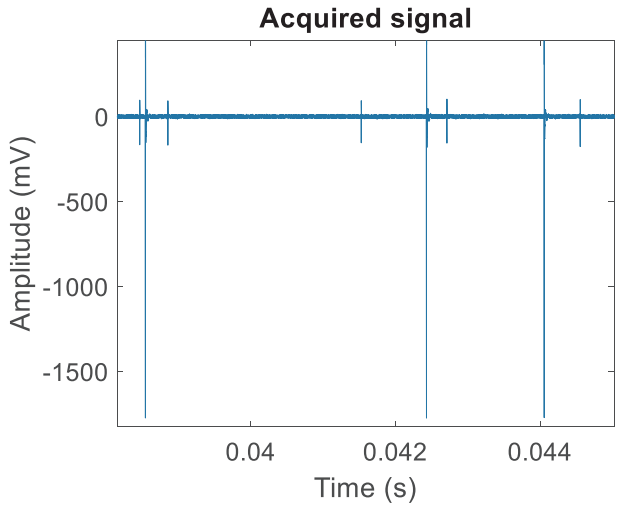

Fig. 15. Discharge stream recorded with the floating electrode defect under positive DC voltage of +29.5 kV_{pk}.

plots of difference in discharge magnitude shown in Fig. 14b. To study the formation of this plot further in detail, the difference in discharge magnitude of successive pulses is plotted in Fig. 16a. The successive bars on the plot depict the difference in charge between two pulses. Observing from Fig. 16a, the magnitude of ΔQ occurs in pairs. For instance, $\Delta Q(1) \approx -\Delta Q(2)$ and $\Delta Q(3) \approx -\Delta Q(4)$. This likeness in magnitudes within the pairs gives rise to the points in cluster 1, while the variation between pairs gives rise to the points over cluster 2 as shown in Fig. 16b. To illustrate this process Fig. 16c shows a sequence of pulses where the first 3 pulses deduce values of ΔQ_i *and* ΔQ_{i+1} that fall in cluster 1 while the consecutive 3, give rise to values that fall in cluster 2. Therefore, the constancy in the discharge magnitude of the smaller pulses and the wide variation in amplitude of the larger pulses forms two distinct clusters in the PSA plot of difference in discharge magnitudes (ΔQ_i *vs.* ΔQ_{i+1}) which could potentially serve in identification of the defect.

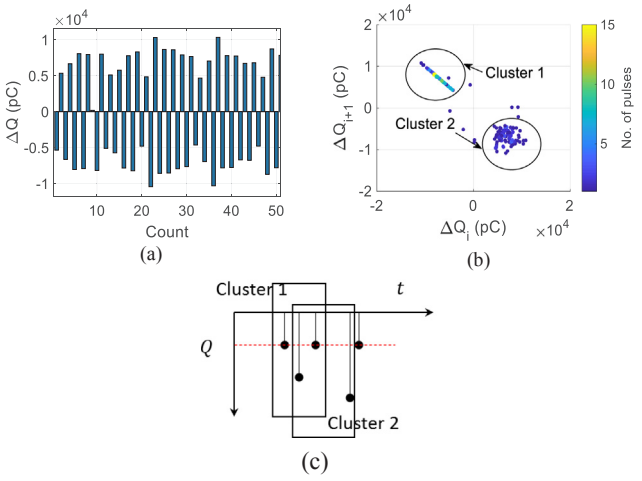

Fig. 16. The formation of the 3 pulse PSA of ΔQ_i *vs.* ΔQ_{i+1} (a) plot of difference in discharge magnitudes of consecutive pulses (b) cluster formation with first 200 pulses and (c) discharge occurrence over time.

5. Conclusions

Floating defects are a rather familiar occurrence while performing HV test. They are identified readily based on their associated PRPD patterns. However, no literature so far has explained the origin of such a pattern. Therefore, this paper illustrates the stepwise progression of the floating discharge defect under AC voltage conditions providing explanation for the pattern's origin. The following important conclusions can be drawn from the study of floating electrode defect on AC stress conditions:

- The phase position of the discharge in one half-cycle of AC voltage is influenced by the phase position of the discharge from the previous half-cycle.
- The discharge from a floating electrode may also appear as a corona pattern on the PRPD diagram depending on the geometry and radius of curvature of the floating object.
- In all cases of the floating electrode defect, on increase voltage, there is an onset of corona over the floating object, given that the healthy part of the dielectric gap does not break leading to complete breakdown/flashover.

In case of DC, though several potential partial discharge patterns had been proposed for PD identification, there has been a lack of knowledge on the discharge progression of a floating electrode defect under DC. This contribution therefore describes in depth the process of discharge of a floating electrode defect and provides a physical interpretation to the derived Pulse Sequence Analysis (PSA) plots yielding some novel and interesting observations. The main contributions of the paper derived based on the study of floating electrode configuration under DC is as follows:

- The discharge process from a floating electrode defect under DC stress differs from AC condition. For the repetitive discharge state, there needs to be alternative occurrence of corona and gap discharge as mentioned in Section 4.1. Otherwise, there is a risk that there is no discharge and the defect is not recognized.
- The results presented in this paper such as the unique pattern in the PSA plot of time between successive discharges in a 3-pulse sequence (Δt_i *vs.* Δt_{i+1}) for the negative DC configuration could potentially serve in the defect's identification. Nevertheless, it provides an extension to the existing knowledge in the field of DC discharge patterns.

CRediT authorship contribution statement

S. Abdul Madhar: Conceptualization, Methodology, Formal analysis, Investigation, Writing - original draft. **P. Mraz:** Writing - review & editing, Supervision, Project administration. **A. Rodrigo Mor:** Writing - review & editing, Supervision, Project administration. **R. Ross:** Supervision.

Declaration of Competing Interest

The authors declare that they have no known competing financial interests or personal relationships that could have appeared to influence the work reported in this paper.

Acknowledgment

This work has received funding from the European Union's Horizon 2020 research and innovation programme under the Marie Sklodowska-Curie grant agreement No. 676042.

References

[1] Roman F, Cooray V, Scuka V. Corona from floating electrodes. J Electrostat 1996;37(1-2):67–78.
[2] Roman F, Lötberg E, Högberg R, Scuka V. Electrical characteristics of insulated metallic bodies in a lightning breakdown field. In: 22nd international conference on lightning protection, ICLP, Budapest, Hungary; 1994.
[3] Roman F. The influence of a floating electrode on the breakdown voltage of a complex gap Licentiate Thesis Institute of High Voltage Research, Uppsala University; 1995
[4] Roman F, Cooray V, Scuka V. The Corona Onset Voltage as a function of the curvature radius of floating electrodes. In: XIth international conference on gas discharges and their applications, Tokyo; 1995.
[5] Hylten-Cavallius N. High voltage laboratory planning. Basel: Emil Hafely & Cie. AG; 1986.
[6] Fruth B, Niemeyer L. The importance of statistical characteristics of partial discharge data. IEEE Trans Electr Insul 1992;27(1):60–9.
[7] Wenger P, Beltle M, Tenbohlen S, Riechert U, Behrmann G. Combined characterization of free-moving particles in HVDC-GIS using UHF PD, high-speed imaging, and pulse-sequence analysis. IEEE Trans Power Delivery 2019;34(4):15.
[8] Gao W, Ding D, Liu W. Research on the typical partial discharge using the UHF detection method for GIS. IEEE Trans Power Delivery 2011;26(4):2621–9.
[9] Standard IEC 60270. High-voltage test techniques–Partial discharge measurements. Int Electrotech Comm 2000.
[10] DDX 9121b Operating Instructions version 7.4, Haefely AG; 2017.
[11] Mor A, Heredia L, Harmsen D, Muñoz F. A new design of a test platform for testing multiple partial discharge sources. Int J Electr Power Energy Syst 2018;94:374–84.
[12] Hoof M, Patsch R. Pulse-sequence analysis: a new method for investigating the physics of PD-induced ageing. IEE Proc – Sci Measure Technol 1995;142(1):95–101.

Saliha Abdul Madhar was born in Chennai, India, in 1994 where she received her Bachelor's in Electrical and Electronics engineering in 2015. She later received her MSc degree in Electrical Sustainable Energy with a special focus on High Voltage techniques, from the Delft University of Technology, the Netherlands, in 2017. She is currently a Marie-Sklodowska Curie Researcher working with Haefely AG in Basel, Switzerland while pursuing her PhD with the Delft University of Technology. Her PhD focusses on the study of Partial Discharge phenomenon under DC stress. Her research interests include HV Asset monitoring and diagnostics and dielectric phenomenon in HVDC.

Petr Mraz received his PhD degree in Diagnosis of Electrical Devices from the University of West Bohemia in Pilsen, Czech Republic in 2014. His research specifically focused on Partial Discharge Measurement and Evaluation. He currently works at Haefely AG, where he started in 2014 as an Application Engineer but has since become a Product Manager and Development Project Leader primarily responsible for Partial Discharge product line. He is a member of several CIGRE working groups and the IEC 60270 maintenance team.

Armando Rodrigo Mor is an Industrial Engineer from Universitat Politècnica de València, in Valencia, Spain, with a Ph.D. degree from this university in electrical engineering. During many years he has been working at the High Voltage Laboratory and Plasma Arc Laboratory of the Instituto de Tecnología Eléctrica in Valencia, Spain. Since 2013 he is an Assistant Professor in the Electrical Sustainable Energy Department at Delft University of Technology, Delft, The Netherlands. His research interests include monitoring and diagnostic, sensors for high voltage applications, high voltage engineering, and HVDC.

Robert Ross is professor at TU Delft, director of IWO (Institute for Science & Development, Ede), professor at HAN University of Applied Sciences and Asset Management Research Strategist at TenneT (TSO in the Netherlands and part of Germany). At KEMA he worked on reliability and post-failure forensic investigations. His interests concern reliability statistics, electro-technical materials, sustainable technology and superconductivity. For energy inventions he was granted a SenterNovem Annual award and nominated Best Researcher by the World Technology Network. He recently wrote the Wiley/IEEE book Reliability Analysis for Asset Management of Electric Power Grids" based on experience with utilities